Nanoscale

RSC Publishing

PAPER

Synergistic effects of the aspect ratio of TiO_2 nanowires and multi-walled carbon nanotube embedment for enhancing photovoltaic performance of dye-sensitized solar cells

Cite this: *Nanoscale*, 2013, **5**, 6842

Ji Young Ahn,[a] Ji Hoon Kim,[a] Kook Joo Moon,[b] So Dam Park[c] and Soo Hyung Kim*[abc]

The existence of numerous interfacial boundaries among TiO_2 nanoparticles (NPs) accumulated in the photoelectrode layer of dye-sensitized solar cells (DSSCs) hinders the effective transport of photogenerated electrons to an electrode. Therefore, as a replacement for TiO_2 NPs, one-dimensional TiO_2 nanowires (NWs) can be suggested to provide pathways for fast electron transport by significantly reducing the number of interfacial boundaries. In order to provide direct evidence for the better performance of such longer TiO_2 NWs than shorter TiO_2 NWs, we examine the effect of the controlled aspect ratio of the TiO_2 NWs randomly accumulated in the photoelectrode layer on the photovoltaic performance of DSSCs. It is clearly found that longer TiO_2 NWs significantly improve the electron transport by reducing the TiO_2/dye/electrolyte interfacial contact resistance. Furthermore, the embedment of multi-walled carbon nanotubes (MWCNTs) as an effective charge transfer medium in longer TiO_2 NWs is proposed in this study to promote more synergistic effects, which lead to significant improvements in the photovoltaic properties of DSSCs.

Received 4th April 2013
Accepted 15th May 2013

DOI: 10.1039/c3nr01689g

www.rsc.org/nanoscale

1 Introduction

Solid TiO_2 nanoparticles (NPs) are generally used as the building blocks for the photoelectrodes in dye-sensitized solar cells (DSSCs).[1] When smaller TiO_2 NPs are used for the photoelectrodes in DSSCs, the resulting photovoltaic performance of the DSSCs is known to be improved.[2–6] This is because the amount of dye adsorption is much larger as a result of their increased specific surface area.[7,8] However, when they are irradiated by sunlight, the transport of the photogenerated electrons injected from the dye molecules is inherently a little slow because of the existence of multiple boundaries among the TiO_2 NPs.[9–11] Therefore, the rapid transport of photogenerated electrons in the TiO_2 NP-accumulated photoelectrode layer is required to improve the photovoltaic performance of DSSCs. Generally, one-dimensional TiO_2 nanowires (NWs) with a high aspect ratio (length-to-diameter ratio, hereafter "AR") can be suggested as a replacement for TiO_2 NPs because they can provide effective pathways for rapid electron transport by reducing the number of interfacial boundaries.[12–20] It has also been reported that the electron diffusion coefficient and electron lifetime are increased when TiO_2 NWs, instead of TiO_2 NPs, are employed in the photoelectrode of DSSCs.[21,22] This implies that the use of longer TiO_2 NWs could promote a higher power conversion efficiency (PCE) in DSSCs as a result of the reduced number of interfacial boundaries. In order to provide direct evidence for the better photovoltaic performance of longer TiO_2 NWs, compared to shorter TiO_2 NWs, length-controlled TiO_2 NWs with a fixed diameter should be fabricated. Then, the effect of the AR of the TiO_2 NWs on the resulting PCE of DSSCs can be easily verified.

Very complex and expensive processes have been used to control the vertical growth and density of a TiO_2 NW (or nanotube) array.[23,24] However, controlling the diameter and length of the TiO_2 NW array was very difficult because of the lack of available template structures.[25] Furthermore, the transport and attachment of a TiO_2 NW array grown from a Ti film (or employing a template-removed medium) to conductive glass as an electrode substrate hinders the application versatility of vertically grown TiO_2 NW arrays. Unlike the previous template-assisted formation of TiO_2 NW arrays, it is possible to easily fabricate TiO_2 NWs using a combination of electrospinning and subsequent calcination processes, in which TiO_2 and polymer precursors are dissolved in a solvent with a relatively high viscosity, and are then turned into TiO_2 NWs by a Coulombic explosion.[26] We employed an electrospinning process, which had the advantages of being simple and cost-effective for

[a]*Department of Nanofusion Technology, Pusan National University, 30 Jangjeon-dong, Geumjung-gu, Busan 609-735, Republic of Korea. E-mail: sookim@pusan.ac.kr; Fax: +82-55-350-5279; Tel: +82-55-350-5672*

[b]*Samsung Electronic Circuit Engineering, Pusan National University, 30 Jangjeon-dong, Geumjung-gu, Busan 609-735, Republic of Korea*

[c]*Department of Nanomechatronics Engineering, Pusan National University, 30 Jangjeon-dong, Geumjung-gu, Busan 609-735, Republic of Korea*

producing massive numbers of TiO_2 NWs. The structures of the resulting electrospun TiO_2 NWs were strongly dependent on various processing parameters.

In this work, the fabrication of diameter- and length-controlled electrospun TiO_2 NWs was demonstrated by varying various parameters, including the polymer molecular weights, the dielectric constant of the base solution used for dissolving the polymer templates, and a subsequent post-ultrasonic process. The effect of the TiO_2 NW structures on the photovoltaic properties of the resulting DSSCs was systematically investigated. Furthermore, the embedment of MWCNTs as an effective charge transfer medium in the TiO_2 matrix NWs with various ARs was made in this study to examine the combination effect of the AR of diameter-controlled TiO_2 NW and MWCNT incorporation with the TiO_2 matrix.

2 Experimental section

2.1 Preparation of TiO_2 NWs and MWCNT-embedded TiO_2 NWs

Various precursors, including titanium isopropoxide (TTIP, Sigma Aldrich), polyvinylpyrrolidone (PVP, Sigma Aldrich, $M_w = 5.5 \times 10^4$ and $M_w = 1.3 \times 10^6$, mp > 300 °C), ethanol (EtOH, absolute, Sigma Aldrich), *N*,*N*-dimethyl-formamide (DMF, Sigma Aldrich), and acetic acid (HAc, 99.7%, Sigma Aldrich), were used for fabricating the TiO_2 NWs without further purification. Three different precursor solutions were prepared as follows: (i) 4.5 g of PVP ($M_w = 5.5 \times 10^4$) dissolved in 10 g of EtOH solution was mixed with 2.5 g of TTIP, (ii) 1.35 g of PVP (Mw $= 1.3 \times 10^6$) dissolved in 8 g of EtOH solution was mixed with 1.44 g of TTIP and 0.576 g of HAc, and (iii) 1.2 g of PVP ($M_w = 1.3 \times 10^6$) dissolved in 8 g of DMF solution was mixed with 1.44 g of TTIP and 0.576 g of HAc. The prepared precursor solutions were then injected at a flow rate of 3 mL h^{-1} using a precision syringe pump (Model no. 78110, KD Scientific). Here, a positive voltage (approximately 25 kV) was applied to the tip of the injection nozzle, while a rotating cylindrical collector was electrically grounded simultaneously. The distance between the injection nozzle tip and the collector was fixed at ~10 cm (see Fig. 1a). The TTIP–PVP composite NWs were then calcined at 450 °C for 3 h to remove the PVP templates.[27] In order to fabricate MWCNT-embedded TiO_2 NWs, MWCNTs were added to the aforementioned PVP–TTIP-mixed solution and then sonicated for 2 h before the electrospinning process. Here, MWCNTs (CNT Co., Korea) with an average diameter of ~20 nm and 15–20 walls were employed as a charge transfer medium inside the TiO_2 matrix NWs without further purification.

2.2 Fabrication of DSSCs

Through a sonication process, the length of the TiO_2 NWs was altered as shown in Fig. 1b. Then, TiO_2 NW-based paste for the screen-printing method was prepared by using EtOH, acetic acid, terpineol (Kanto Chemical), ethyl cellulose (Sigma Aldrich), and N-719 (Solaronix) for the dye solution; AN-50 (Solaronix) for the liquid electrolyte; and fluorine-doped tin oxide (FTO, 7 Ω sq^{-1}, Pilkington) glass. First, 6 g of the TiO_2 NWs was dispersed in a mixture of 15 g of EtOH and 1 mL of acetic acid by using an ultrasonicator operated at 200 W and 40 kHz for 30 min. Second, 20 g of terpineol was added to the TiO_2 NW solution and 3 g of ethyl cellulose was dissolved in 27 g of EtOH. Finally, the two prepared solutions were homogeneously mixed by using an ultrasonicator for 30 min, and then heated at 80 °C to evaporate the residual solvents. The prepared TiO_2 NW paste was then coated on the FTO glass (2 cm × 2 cm) using a screen-printing method. The FTO glass was thermally treated at 500 °C for 30 min after pretreatment with a solution of 0.247 mL of $TiOCl_2$ and 20 mL of deionized water to enhance the adhesion between the TiO_2 NW layer and the FTO glass. The TiO_2 NW-coated FTO glass was then sintered at 500 °C for 30 min to remove the residual components. The resulting TiO_2 NW-coated FTO glass was then soaked in a dye solution for 24 h, while another FTO glass as a counter electrode was sputtered with Pt. Both the photoelectrode and the counter electrode were then sealed with a hot-melt film (60 μm thickness, Surlyn, DuPont) heated at 120 °C for 3 min. The assembly of a DSSC unit was finally completed after injecting the iodide-based liquid electrolyte (AN-50, Solaronix), as shown in Fig. 1c.

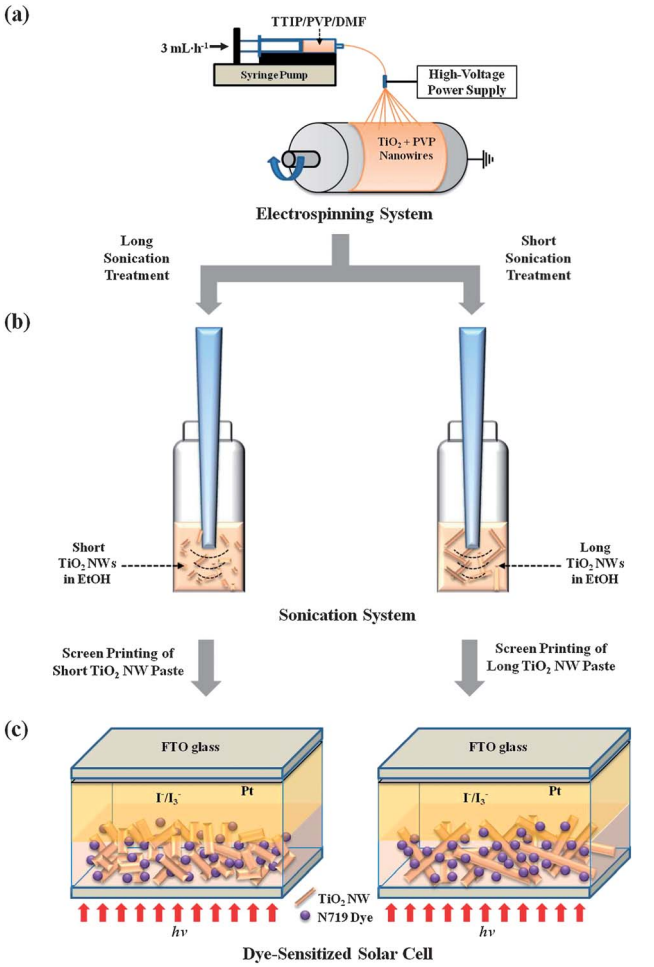

Fig. 1 Schematics of the (a) electrospinning process, (b) sonication process, and (c) DSSCs composed of TiO_2 NWs with various aspect ratios (ARs).

2.3 Characterization

The fabricated electrospun TiO_2 NWs were characterized using a field-emission scanning electron microscope (FE-SEM, S4700, Hitachi) operated at 15 kV, transmission electron microscope (TEM, JEM 2100F, JEOL) operated at ~100 kV, and X-ray diffraction (XRD, Empyrean series2, PANalytical). The photovoltaic properties of the DSSCs fabricated in this study were characterized using a solar simulator (PEC-L12, Pecell Technologies Inc.) under AM 1.5 and 1 sun (= 100 mW cm^{-2}) illumination. The intensity of the sunlight illumination was calibrated using a standard Si photodiode detector with a KG-5 filter. The current density–voltage (J–V) curves were recorded automatically with a Keithley SMU 2400 source meter by illuminating the DSSCs.

3 Results and discussion

Various operating parameters, including the polymer types, solution property, applied voltage, and injection rate of the precursor solution, can strongly affect the diameter of the electrospun TiO_2 NWs. At a fixed applied voltage and injection rate for the precursor solution, we mainly perturbed the polymer molecular weight and solution property to control the diameter of the electrospun TiO_2 NWs in this approach. First, two groups of electrospun TiO_2–PVP composite NWs were prepared by mixing TTIP with PVP, which had two different molecular weights (M_w = 5.5 × 10^4 and 1.3 × 10^6). The SEM images in Fig. 2a and c show the as-prepared TiO_2–PVP composite NWs, indicating that the average diameter of the TiO_2–PVP composite NWs decreased slightly with an increase in the initial polymer molecular weight. After removal of the PVP templates by calcination at 450 °C, the average diameter of the resulting TiO_2 NWs was accordingly decreased from 168 ± 33 nm (Fig. 2b) to 145 ± 33 nm (Fig. 2d). As another approach, we simply changed the EtOH into DMF for dissolving the TiO_2/PVP precursors to observe the effect of the solution property on the structural change in the resulting TiO_2 NWs. Here, it should be noted that the dielectric constants were ~24.3 and ~37.6 for EtOH and DMF, respectively.[28,29] The as-prepared TiO_2–PVP composite NWs with the same initial polymer concentrations dissolved in EtOH and DMF solvents, respectively, are shown in Fig. 2c and e. The average diameter of the TiO_2–PVP composite NWs was clearly observed to decrease when employing DMF, which had a higher dielectric constant than EtOH; this suggests that the TiO_2/PVP precursors were polarized more in the DMF than in the EtOH, which allowed the ejected jet of TiO_2/PVP precursors at the electrospinning nozzle tip to carry higher charges. Thus, stronger electrostatic repulsion forces were induced to form TiO_2–PVP composite NWs with smaller diameters. It can clearly be seen that the average diameter of the resulting TiO_2 NWs decreased from 145 ± 33 nm (Fig. 2d) to 65 ± 3 nm (Fig. 2f) after a calcination process at 450 °C performed to remove the PVP templates.

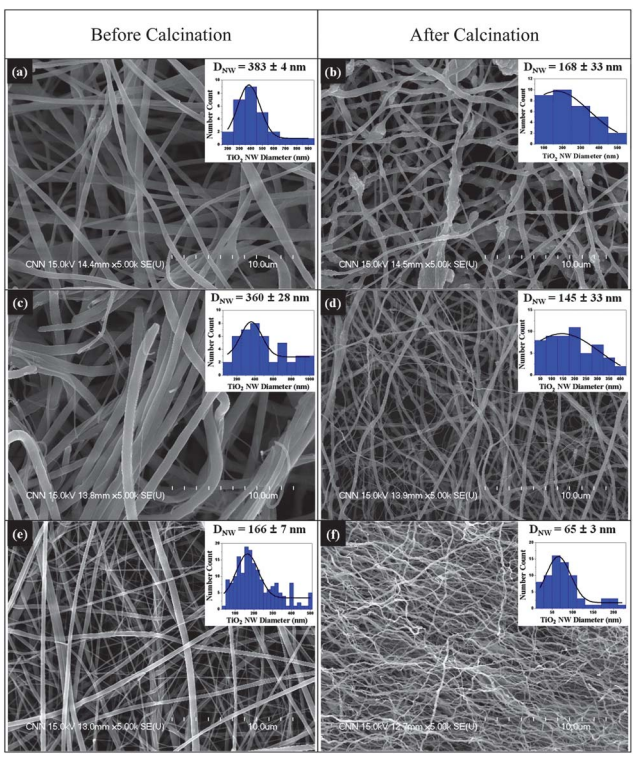

Fig. 2 SEM images of (i) TiO_2/PVP NWs prepared using TTIP/PVP (M_w = 5.5 × 10^4)/EtOH (a) before and (b) after calcination at 450 °C, (ii) TiO_2/PVP NWs prepared using TTIP/PVP (M_w = 1.3 × 10^6)/EtOH (c) before and (d) after calcination at 450 °C, and (iii) TiO_2/PVP NWs prepared using TTIP/PVP (M_w = 1.3 × 10^6)/DMF (e) before and (f) after calcination at 450 °C.

Fig. 3 shows the XRD patterns of various TiO_2 NWs before and after calcination at 450 °C. As-electrospun PVP/TiO_2 NWs prior to calcination at 450 °C were found to be amorphous structures as shown in Fig. 3(a-1). However, after calcination at 450 °C, the resulting phase composition of TiO_2 NWs fabricated by this approach was determined to be anatase : rutile = 60 : 40 TTIP/PVP(M_w = 1.3 × 10^6)/DMF (Fig. 3(a-2)), 47 : 53 for TTIP/PVP(M_w = 1.3 × 10^6)/EtOH (Fig. 3(a-3)), and 54 : 46 for TTIP/PVP(M_w = 5.5 × 10^4)/EtOH cases (Fig. 3(a-4)), respectively, suggesting that there was no appreciable change in the phase compositions of the resulting TiO_2 NWs. The phase composition was calculated from the integrated intensities of the anatase and rutile peaks.

In order to investigate the effect of the AR of the TiO_2 NWs on the photovoltaic performance of the DSSCs, we needed to obtain TiO_2 NWs with different length distributions. Thus, the average diameter of the TiO_2 NWs was fixed at ~145 ± 33 nm, and their length was altered by using sonication energy, as shown in the schematic of Fig. 1b. Before controlling the TiO_2 structures, we first performed more XRD analyses for the TiO_2 NWs (*i.e.*, TTIP/PVP(M_w = 1.3 × 10^6)/DMF case) treated for different sonication times from 1 to 180 min. As shown in the results, there were no appreciable changes in the strong signal peaks corresponding to the anatase and rutile structures. The mixing ratios of phase compositions were anatase : rutile = 60 : 40 for 1 min sonication (Fig. 3(b-1)), anatase : rutile = 55 : 45 for 30 min sonication (Fig. 3(b-2)), anatase : rutile = 51 : 49 for 120 min sonication (Fig. 3(b-3)), and anatase : rutile = 50 : 50 for 180 min sonication (Fig. 3(b-4)), respectively. It suggests that the sonication time cannot strongly affect the phase change of TiO_2 NWs.

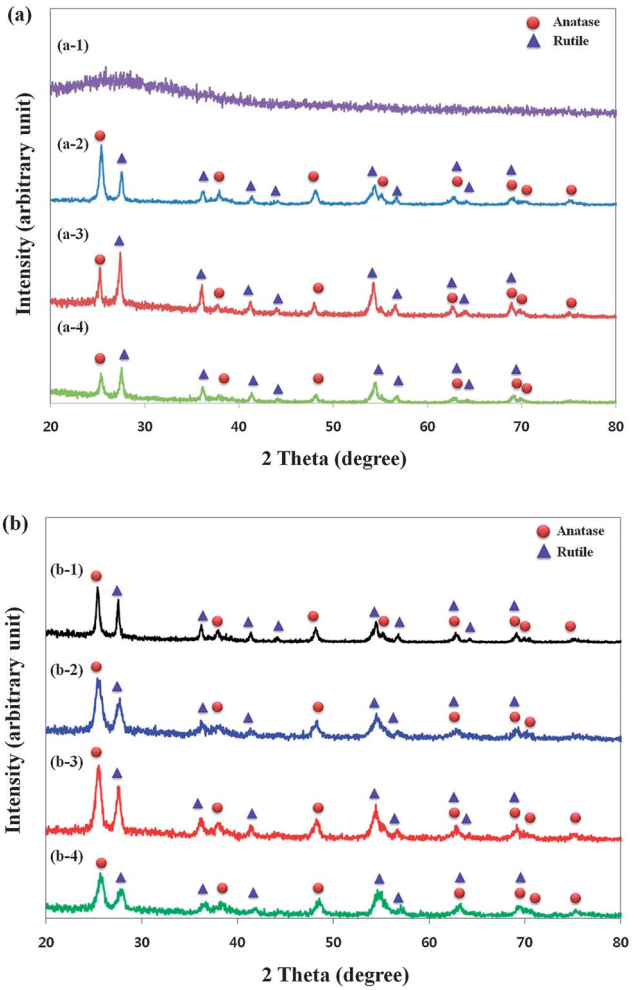

Fig. 3 XRD spectra of as-electrospun TiO_2 NWs fabricated by TTIP/PVP(M_w = 1.3 × 10^6)/DMF (a-1) before and (a-2) after calcination at 450 °C. XRD spectra of as-electrospun TiO_2 NWs fabricated by (a-3) TTIP/PVP(M_w = 1.3 × 10^6)/EtOH and (a-4) TTIP/PVP(M_w = 5.5 × 10^4)/EtOH after calcination at 450 °C. XRD spectra of TiO_2 NWs fabricated by TTIP/PVP(M_w = 1.3 × 10^6)/DMF after calcination at 450 °C and subsequent sonication treatment for (b-1) 1, (b-2) 30, (b-3) 120 and (b-4) 180 min.

The SEM images and length distributions of the TiO_2 NWs as a function of the sonication time (t_s) are shown in Fig. 4a–e. The AR of the resulting TiO_2 NWs was varied from ~7 (t_s = 300 min, L_{NW} = ~1.00 μm, Fig. 4d) to ~90 (t_s = 1 min, L_{NW} = ~12.57 μm, Fig. 4a). Here, we can obtain the longest TiO_2 NWs with the AR of ~90 after sonication for ~1 min, which is the minimum requirement to obtain well-dispersed TiO_2 NWs in solvent for the preparation of TiO_2 paste later. It is apparent that the average length of the TiO_2 NWs decreased significantly with an increase in the intensive sonication time as shown in Fig. 4e. This suggests that the sonication energy sufficiently induced the destruction and shortening of the TiO_2 NWs. Here, a question arises: can the length of TiO_2 NWs with a fixed diameter strongly affect the resulting specific surface area of TiO_2 NWs? To find an answer for the question, nitrogen gas adsorption analysis of TiO_2 NWs with different ARs was performed as shown in Fig. 4f. It indicates that the gas volume adsorbed on the surface of TiO_2 NWs and the resulting specific surface area (S_{BET}) of TiO_2 NWs were not appreciably changed by varying the AR of TiO_2 NWs. Therefore, shortening of the diameter-controlled TiO_2 NWs does not seem to significantly perturb the available surface area for absorbing dye molecules later in the DSSCs, but it simply increases the number of boundaries among TiO_2 NWs.

In order to examine the effect of the AR of the TiO_2 NWs on the photovoltaic properties of DSSCs, we fabricated various groups of DSSCs composed of TiO_2 NWs with different ARs. Fig. 5a and b show the SEM images of the top and side views of TiO_2 NWs randomly accumulated on the surface of the FTO glass. The average thicknesses of the long and short TiO_2 NW-accumulated photoelectrode layers were found to be similar at approximately 22 μm. Fig. 5c shows a photograph of a DSSC unit cell with a 6 mm × 6 mm photoactive area. Fig. 5d and Table 1 summarize the current density–voltage (J–V) curves and the photovoltaic performance of DSSCs measured under AM 1.5 illumination (100 mW cm^{-2}), respectively. It was clearly observed that the short circuit current density (J_{sc}) increased with an increase in the AR of the TiO_2 NWs, as shown in Fig. 5d. The J_{sc} values of the DSSCs composed of TiO_2 NWs increased from 0.91 ± 0.08 mA cm^{-2} for AR = ~7 (L_{NW} = ~0.96 μm) to 4.14 ± 0.32 mA cm^{-2} for AR = ~90 (L_{NW} = ~12.57 μm), resulting in a considerable improvement in the PCE from 0.42 ± 0.02% to 2.02 ± 0.15%, respectively. This suggests that longer TiO_2 NWs become a rapid and effective transport medium for photogenerated electrons compared to shorter TiO_2 NWs because of the significant reduction in the number of interfacial boundaries among the TiO_2 NWs.

This was also corroborated by electrochemical impedance spectroscope (EIS) measurements to identify the charge-transfer-related internal resistance of the TiO_2 NW-based photoelectrodes, as shown in Fig. 6. The Nyquist plot in Fig. 6a shows that longer TiO_2 NWs reduced the charge transfer resistance at the TiO_2 NW/dye/electrolyte interfaces. The photogenerated electrons could diffuse and transport more rapidly through the longer TiO_2 NWs, which resulted in a lower resistance and higher PCE, as shown in Fig. 6a and Table 1. Fig. 6b shows Bode phase plots for analyzing the electron lifetime. The maximum frequency shifted to a higher value with a decrease in the AR of the TiO_2 NWs, and the electron lifetime ($\tau = [2\pi f_{max}]^{-1}$, where f_{max} is the maximum frequency) was calculated to be decreased from 1.9 ms (AR = ~90) to 0.5 ms (AR = ~7), suggesting that the photogenerated electrons could diffuse further along the longer TiO_2 NWs than along the shorter TiO_2 NWs. It should also be noted in Table 1 that both the open circuit voltage (V_{oc}) and the fill factor (FF) of the DSSCs did not show any appreciable changes, suggesting that the photovoltaic conversion properties and interfacial structures of the TiO_2 NW-based photoelectrode layer and liquid electrolyte were very similar for all of the DSSCs assembled with various TiO_2 NWs in this approach.

There are possibilities that an increase of J_{sc} value in DSSCs can also occur due to the differences in the total amount of dye adsorption and the magnitude of light scattering in the photoelectrode employed TiO_2 NWs with various ARs. First, in order to examine the relative amount of dye adsorption for the DSSCs

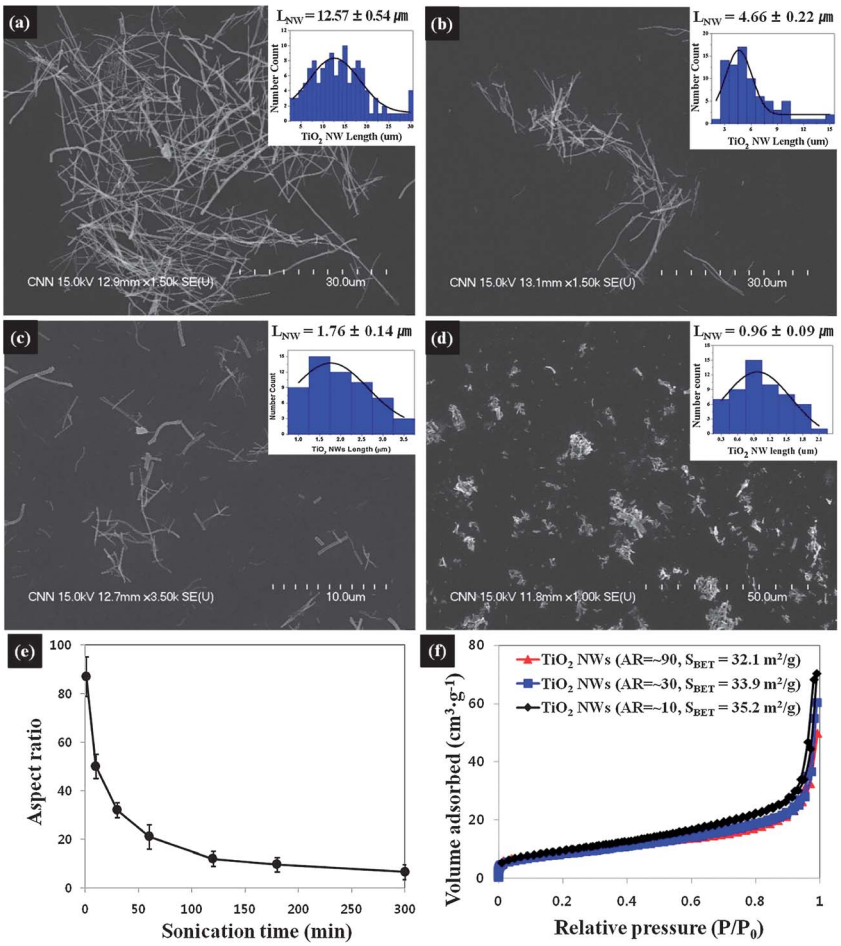

Fig. 4 SEM images of TiO_2 NWs after sonication for (a) 1, (b) 30, (c) 120, and (d) 300 min (L_{NW} is the average length of TiO_2 NWs). (e) Aspect ratio of TiO_2 NWs as a function of sonication time, and (f) nitrogen adsorption and desorption curves for TiO_2 NWs with various ARs.

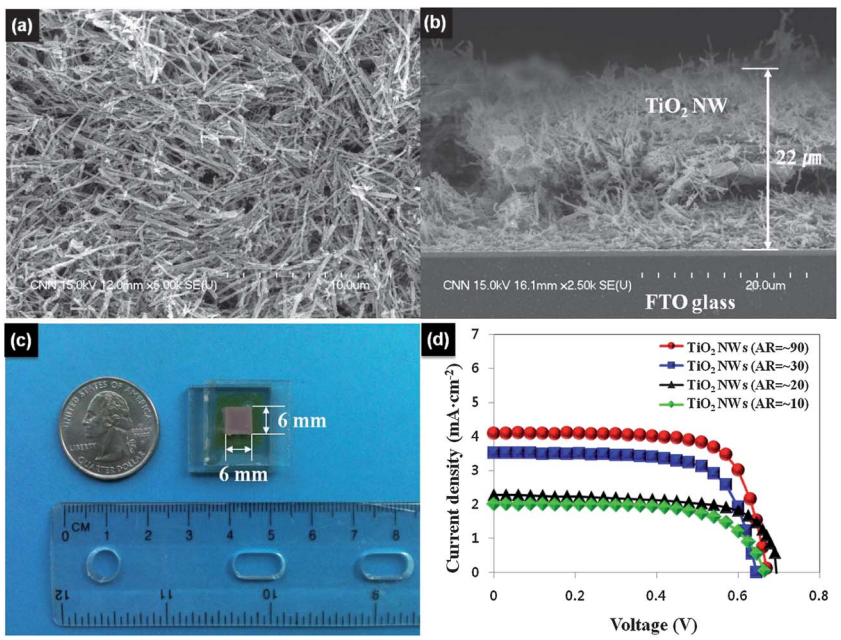

Fig. 5 SEM images of (a) top and (b) side views of the TiO_2 NW-accumulated photoelectrode (AR = ~30), (c) photograph of the assembled DSSC unit cell, and (d) *J–V* curves of DSSCs composed of TiO_2 NWs with different ARs.

Table 1 Summary of photovoltaic characteristics of TiO_2 NW-accumulated DSSCs[a]

t_s [min]	L_{NW} [μm]	AR	τ_e [ms]	M_{DA} [10^{-7} mol cm^{-2}]	J_{sc} [mA cm^{-2}]	V_{oc} [V]	FF	PCE [%]
1	12.57 ± 0.54	86.69 ± 3.72	1.9	1.05	4.14 ± 0.32	0.67 ± 0.02	0.73 ± 0.02	2.02 ± 0.15
10	7.16 ± 0.41	49.38 ± 2.83	1.3	1.03	3.79 ± 0.25	0.65 ± 0.01	0.72 ± 0.01	1.77 ± 0.12
30	4.66 ± 0.22	32.14 ± 1.52	1.2	1.03	3.49 ± 0.17	0.65 ± 0.01	0.72 ± 0.01	1.63 ± 0.08
60	3.04 ± 0.11	20.97 ± 0.76	1.0	1.01	2.58 ± 0.37	0.64 ± 0.01	0.71 ± 0.01	1.17 ± 0.16
120	1.76 ± 0.14	12.14 ± 0.97	0.8	1.09	2.00 ± 0.07	0.67 ± 0.01	0.67 ± 0.01	0.90 ± 0.13
180	1.41 ± 0.07	9.72 ± 0.48	0.7	1.06	1.79 ± 0.11	0.67 ± 0.02	0.69 ± 0.01	0.83 ± 0.06
300	0.96 ± 0.09	6.62 ± 0.62	0.5	1.02	0.91 ± 0.08	0.68 ± 0.01	0.68 ± 0.01	0.42 ± 0.02

[a] t_s = sonication time; L_{NW} = average length of the TiO_2 NW; AR = aspect ratio of the TiO_2 NW; τ_e = electron lifetime; M_{DA} = amount of dye absorbed; J_{sc} = short circuit current density; V_{oc} = open circuit voltage; FF = fill factor; PCE = power conversion efficiency.

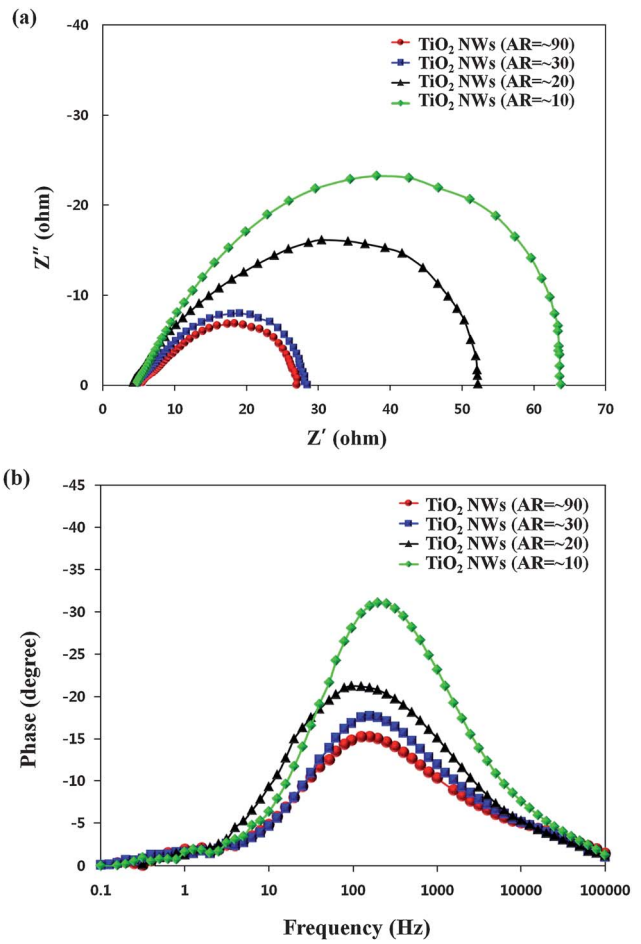

Fig. 6 (a) Nyquist plots and (b) Bode plots of various DSSCs composed of TiO_2 NWs with different ARs.

fabricated in this approach, UV-Vis measurements were performed for dye-dissolved NaOH solutions collected from the photoelectrodes composed of TiO_2 NWs with various ARs as shown in Table 1. The total amount of dye adsorbed on the surface of TiO_2 NWs with various ARs ranging from ~7 to ~90 was found to be 1.01×10^{-7} to 1.09×10^{-7} mol cm^{-2}, suggesting that the difference of the total amount of dye adsorbed in the photoelectrodes of DSSCs fabricated in this approach was negligibly small. This result is also consistent with the BET measurement for various TiO_2 NWs as shown in Fig. 4f. Second, the reflectance of the various TiO_2 NW-accumulated photoelectrodes was also examined to verify the light-scattering capability as shown in Fig. 7. Three different DSSCs composed of TiO_2 NWs with ARs of 10, 30, and 90 exhibited very similar reflectance in the wavelength range of 300–800 nm, suggesting that the TiO_2 NWs with different ARs fabricated in this approach did not show much appreciable change in the magnitude of light-scattering. Therefore, the increase of J_{sc} in the DSSCs composed of longer TiO_2 NWs mostly occurs by the reduction of the number of interfacial boundaries among the given longer TiO_2 NWs.

In order to inherently improve the photovoltaic performance of the TiO_2 NW-accumulated DSSCs, we propose a viable method, in which MWCNTs were added to the TiO_2 NWs during the electrospinning process. Here, MWCNTs were employed as an effective charge transfer medium for the fast transport of photogenerated electrons inside the TiO_2 matrix NWs. A closer look at a single MWCNT-embedded TiO_2 NW, as shown in the SEM images of Fig. 8a and b, shows that the MWCNTs were axially aligned along a TiO_2 matrix NW. Unlike the SEM images,

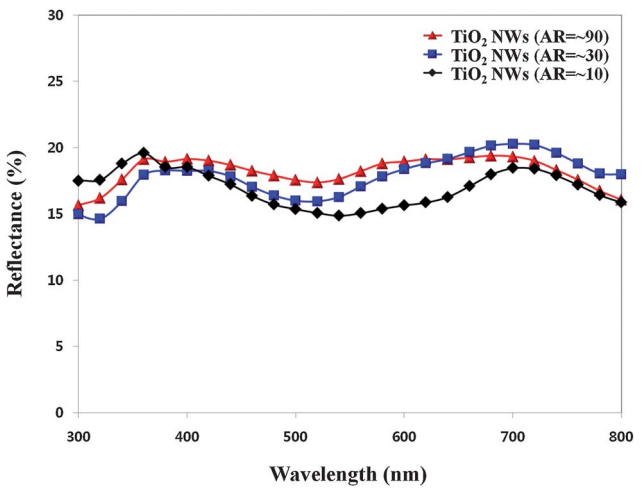

Fig. 7 UV-Vis measurement of various TiO_2 NW-accumulated photoelectrode layers.

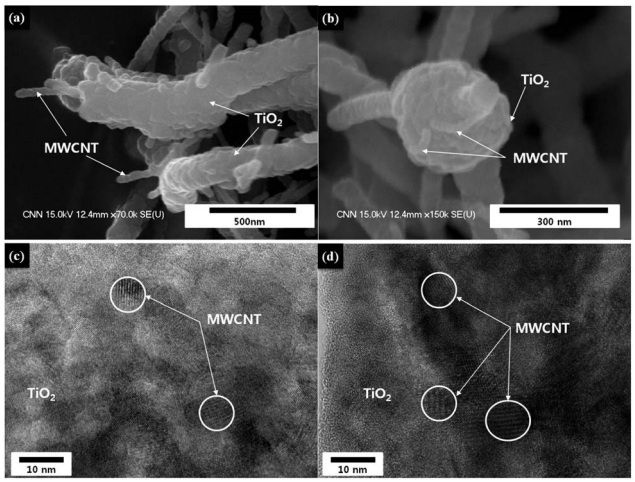

Fig. 8 (a and b) SEM images and (c and d) HRTEM images of the thin layer of MWCNT-embedded TiO_2 NWs prepared by using a focused ion beam (FIB).

the presence of MWCNTs in the TiO_2 NWs was not clearly observed in TEM images because of the relatively high transmittance of electrons in the MWCNTs. However, the high-resolution TEM (HRTEM) image for the thin film of an MWCNT-embedded TiO_2 NW sample prepared using a focused ion beam (FIB), as shown in Fig. 8c and d, confirmed that the MWCNTs clearly resided inside the TiO_2 matrix NW.

Table 2 summarizes the photovoltaic characteristics of the MWCNT (5 wt%)–TiO_2 composite NW-accumulated DSSCs. It can clearly be observed that the embedment of MWCNTs (5 wt%) into the TiO_2 NWs significantly improved the J_{sc} and PCE of the DSSCs, suggesting that the MWCNTs played a key role as an effective charge transfer medium in the TiO_2 NWs. It was also confirmed that the use of longer MWCNT–TiO_2 composite NWs improved the PCE of the DSSCs compared to shorter MWCNT–TiO_2 composite NWs. The PCE value increased from 2.88 ± 0.23% (AR = ~7) to 5.16 ± 0.24% (AR = ~90). Here, we have measured the PCE of DSSCs as a function of the amount of MWCNTs in the TiO_2 NWs as shown in Fig. 9a. As the amount of MWCNTs increased up to ~5 wt%, the maximum PCE of DSSCs was obtained. However, a much larger amount of MWCNT inclusion (>10 wt%) in the TiO_2 NWs resulted in lowering of the PCE of DSSCs due to charge recombination caused by the exfoliation of highly aggregated MWCNTs in the TiO_2 matrix such that photogenerated electrons are easily lost by contact with the liquid electrolyte.

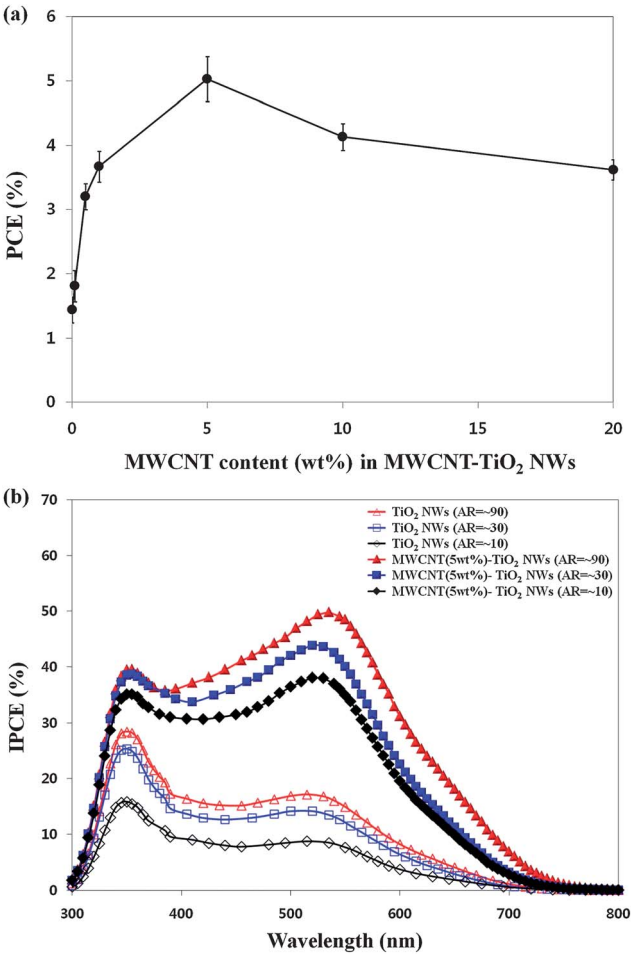

Fig. 9 (a) The evolution of PCE of DSSCs as a function of MWCNT content in MWCNT–TiO_2 NWs and (b) the IPCE spectra of DSSCs with pure TiO_2 NWs or MWCNT–TiO_2 composite NWs with various ARs.

To understand the major factor leading to the improvement in PCE in the longer TiO_2 NW-accumulated DSSCs, incident photon-to-electron conversion efficiency (IPCE) spectra were recorded as a function of the incident light wavelength. The IPCE spectra as shown in Fig. 9b show that longer TiO_2 NW-accumulated DSSCs exhibited better IPCE than the shorter TiO_2 NW-accumulated DSSCs, suggesting that the longer TiO_2 NWs possess a more effective light-harvesting capacity. The relative magnitude of the IPCE spectra for MWCNT–TiO_2 composite NW-accumulated DSSCs was much higher than

Table 2 Summary of photovoltaic characteristics of MWCNT (5 wt%)–TiO_2 composite NW-accumulated DSSCs

t_s [min]	L_{NW} [μm]	AR	τ_e [ms]	M_{DA} [10^{-7} mol cm^{-2}]	J_{sc} [mA cm^{-2}]	V_{oc} [V]	FF	PCE [%]
1	12.76 ± 0.20	88.00 ± 1.38	5.0	1.07	9.91 ± 0.35	0.72 ± 0.01	0.71 ± 0.01	5.16 ± 0.24
10	8.17 ± 0.35	56.34 ± 2.41	4.1	1.08	9.59 ± 0.19	0.72 ± 0.02	0.69 ± 0.01	4.79 ± 0.18
30	4.24 ± 0.26	29.24 ± 1.79	3.1	1.05	8.41 ± 0.23	0.70 ± 0.01	0.74 ± 0.01	4.36 ± 0.11
60	3.23 ± 0.22	22.28 ± 1.52	2.5	1.06	7.70 ± 0.04	0.69 ± 0.01	0.74 ± 0.01	3.94 ± 0.05
120	1.85 ± 0.04	12.69 ± 0.28	2.0	1.05	7.16 ± 0.16	0.66 ± 0.01	0.69 ± 0.01	3.24 ± 0.09
180	1.43 ± 0.08	9.86 ± 0.55	1.8	1.07	6.59 ± 0.22	0.69 ± 0.01	0.70 ± 0.01	3.18 ± 0.04
300	0.95 ± 0.04	6.55 ± 0.28	1.5	1.04	6.05 ± 0.17	0.67 ± 0.01	0.71 ± 0.01	2.88 ± 0.23

those for pure TiO_2 NW-accumulated DSSCs, confirming that the MWCNTs embedded in the TiO_2 matrix NWs play the role as an effective charge transfer medium for inherently enhancing the photovoltaic performance of DSSCs.

From the various direct observations, we can infer that longer TiO_2 NWs are more effective than shorter TiO_2 NWs in transferring photogenerated electrons, because longer TiO_2 NWs reduce the number of interfacial boundaries among the TiO_2 structures. Longer MWCNT–TiO_2 composite NWs in the photoelectrodes also reduce electron recombination and simultaneously accelerate electron transfer. It is because the MWCNTs embedded in the longer TiO_2 NWs rapidly absorb the photogenerated electrons, and then transfer them through the TiO_2 matrix toward FTO glass substrates as shown in Fig. 10. The values of J_{sc} and V_{oc} increased from 4.14 mA cm^{-2} and 0.67 V for TiO_2 NW (AR = ~90)-accumulated DSSCs to 9.91 mA cm^{-2} and 0.72 V for MWCNT (5 wt%)–TiO_2 composite NW (AR = ~90)-accumulated DSSCs (see Tables 1 and 2). The increase of J_{sc} value occurred due to the presence of MWCNTs as an effective charge transfer medium in MWCNT–TiO_2 composite NW-accumulated DSSCs also results in an increase in the V_{oc} value. This is consistent with the general theoretical model given in eqn (1) for conventional inorganic solar cells, and also can be confirmed by the increase of J_{sc} and V_{oc} values in MWCNT–TiO_2 composite NW-accumulated DSSCs compared to those of TiO_2 NW-accumulated DSSCs.

$$V_{oc} \approx \frac{nkT}{q} \ln\left(\frac{J_{sc}}{J_o}\right) \quad (1)$$

where n is the diode quality factor, k is the Boltzmann constant, T is the absolute temperature, q is the electronic charge, J_{sc} is the short circuit current density, and J_o is the reverse saturation current density.

The higher V_{oc} in MWCNT–TiO_2 composite NW-accumulated DSSCs can also be confirmed by the EIS analysis results. The electron lifetime (τ_e) determined as inversely proportional to the maximum frequency (*i.e.*, $\tau_e = (2\pi f_{max})^{-1}$, where f_{max} is the maximum frequency of the middle-frequency peak in the Bode phase plot) in the middle range of Bode phase plots for MWCNT(5 wt%)–TiO_2 composite NW-accumulated DSSCs is much longer than that for TiO_2 NW-based DSSCs. (The τ_e value is increased from 1.9 ms for TiO_2 NW (AR = ~90)-accumulated DSSC to 5 ms for MWCNT–TiO_2 (AR = ~90)-accumulated DSSCs as shown in Tables 1 and 2.) The V_{oc} values are also known to be proportional to $\ln(1/f_{max})$, which indicates that the V_{oc} can be significantly affected by the charge recombination.[30] The exfoliation of MWCNTs and the number of interfacial boundaries are increased by shortening the TiO_2 NWs; thus, the photogenerated electrons are easily lost by contact with the electrolyte, dye, and TiO_2 (see Fig. 10), which eventually resulted in significant reduction of photovoltaic performance of DSSCs.

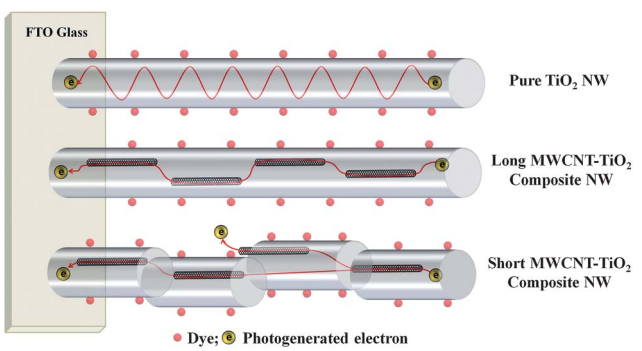

Fig. 10 Schematic of charge transfer in the pure TiO_2 NW or MWCNT–TiO_2 composite NW with different ARs.

4 Conclusions

We investigated the effect of the number of interfacial boundaries among TiO_2 nanostructures on the photovoltaic performance of DSSCs. In order to control the number of interfacial boundaries in a given mass of TiO_2 nanostructure-based paste, the AR of electrospun TiO_2 NWs with a fixed average diameter (~145 nm) was varied from ~7 to ~90 using a post-sonication process. As a result, the photovoltaic performance of the DSSCs with longer TiO_2 NWs was improved by the presence of a smaller number of interfacial boundaries. This was also confirmed by an EIS analysis, in which the TiO_2/dye/electrolyte internal resistance was observed to have been decreased significantly with an increase in the AR of the TiO_2 NWs. The embedment of MWCNTs as an effective charge transfer medium in the TiO_2 matrix NWs was also proposed to inherently improve the photovoltaic performance of the DSSCs. The resulting PCE of the DSSCs increased from 2.02 ± 0.15% (*i.e.*, w/o MWCNT addition) to a maximum of 5.16 ± 0.24%, which resulted from the addition of MWCNTs (5 wt%) into the longest TiO_2 matrix NW (AR = ~90)-based paste in this study. This also confirmed that semiconducting nanostructures with a higher AR and enhanced electrical conductivity can significantly improve the inherent photovoltaic performance of DSSCs by rapid and efficient electron transfer.

Acknowledgements

This study was supported by the National Research Foundation of Korea (NRF) funded by the Korean government (MEST) (2011-0013114).

References

1 B. O'Regan and M. Grätzel, *Nature*, 1991, **353**, 737–739.
2 A. Kay and M. Grätzel, *Sol. Energy Mater. Sol. Cells*, 1996, **44**, 99–117.
3 M. Durr, A. Schmid, M. Obermaier, S. Rossolli, A. Yasuda and G. Nellesm, *Nat. Mater.*, 2005, **4**, 607–611.
4 S. Nakade, M. Matsuda, S. Kambe, Y. Saito, T. Kitamura, T. Sakata, Y. Wada, H. Mori and S. Yanagida, *J. Phys. Chem. B*, 2002, **106**, 10004–10010.
5 J. Yu, J. Fan and B. Cheng, *J. Power Sources*, 2011, **196**, 7891–7898.
6 C.-R. Ke and J.-M. Ting, *J. Power Sources*, 2012, **208**, 316–321.
7 Z. S. Wang, H. Kawauchi, T. Kashima and H. Arakawa, *Coord. Chem. Rev.*, 2004, **248**, 1381–1389.

8 T. Lopez-Luke, A. Wolcott, L. P. Xu, S. W. Chen, Z. H. Wen, J. H. Li, E. De La Rosa and J. Z. Zhang, *J. Phys. Chem. C*, 2008, **112**, 1282–1292.

9 M. Law, L. E. Greene, J. C. Johnson, R. Saykally and P. D. Yang, *Nat. Mater.*, 2005, **4**, 455–459.

10 D. Chen, H. Zhang, S. Hu and J. Li, *J. Phys. Chem. C*, 2008, **112**, 117–122.

11 K. Zhu, N. R. Neale, A. Miedaner and A. J. Frank, *Nano Lett.*, 2007, **7**, 69–74.

12 S. R. Jang, R. Vittal and K. J. Kim, *Langmuir*, 2004, **20**, 9807–9810.

13 Y. B. Tang, C. S. Lee, J. Xu, Z. T. Liu, Z. H. Chen, Z. B. He, Y. L. Cao, G. D. Yuan, H. S. Song, L. M. Chen, L. B. Luo, H. M. Cheng, W. J. Zhang, I. Bello and S. T. Lee, *ACS Nano*, 2010, **4**, 3482–3488.

14 H. Hayashi, I. V. Lightcap, M. Tsujimoto, M. Takano, T. Umeyama, P. V. Kamat and H. Imahori, *J. Am. Chem. Soc.*, 2011, **133**, 7684–7687.

15 P. V. Kamat, *J. Phys. Chem. Lett.*, 2011, **2**, 242–251.

16 P. V. Kamat, K. Tvrdy, D. R. Baker and J. G. Radich, *Chem. Rev.*, 2010, **110**, 6664–6688.

17 S. Zhang, H. Niu, Y. Lan, C. Cheng, J. Xu and X. Wang, *J. Phys. Chem. C*, 2011, **115**, 22025–22034.

18 X. Dang, H. Yi, M.-H. Ham, J. Qi, D. S. Yun, R. Ladewski, M. S. Strano, P. T. Hammond and A. M. Belcher, *Nat. Nanotechnol.*, 2011, **6**, 377–384.

19 W. Guo, C. Xu, X. Wang, S. Wang, C. Pan, C. Lin and Z. L. Wang, *J. Am. Chem. Soc.*, 2012, **134**, 4437–4441.

20 J. Chen, B. Li, J. Zheng, J. Zhao and Z. Zhu, *J. Phys. Chem. C*, 2012, **116**, 14848–14856.

21 T. Krishnamoorthy, V. Thavasi, M. Subodh and S. Ramakrishna, *Energy Environ. Sci.*, 2011, **4**, 2807–2812.

22 Z. Zhou, J. Fan, X. Wang, W. Zhou, Z. Du and S. Wu, *ACS Appl. Mater. Interfaces*, 2011, **3**, 4349–4353.

23 M. Ye, X. Xin, C. Lin and Z. Lin, *Nano Lett.*, 2011, **11**, 3214–3220.

24 J. Lin, X. Liu, M. Guo, W. Lu, G. Zhang, L. Zhou, X. Chen and H. Hung, *Nanoscale*, 2012, **4**, 5148–5153.

25 F. Shao, J. Sun, L. Gao, S. Yang and J. Luo, *J. Phys. Chem. C*, 2011, **115**, 1819–1823.

26 R. Chandrasekar, L. Zhang, J. Y. Howe, N. E. Hedin, Y. Zhang and H. Fong, *J. Mater. Sci.*, 2009, **44**, 1198–1205.

27 J. Y. Ahn, W. D. Kim, K. Cho, D. G. Lee and S. H. Kim, *Powder Technol.*, 2011, **211**, 65–71.

28 D. H. Reneker and I. Chun, *Nanotechnology*, 1996, **7**, 216–223.

29 A. Frenot and I. S. Chronakis, *Curr. Opin. Colloid Interface Sci.*, 2003, **8**, 64–75.

30 D. Hwang, S. M. Jo, D. Y. Kim, V. Armel, D. R. MacFarlane and S.-Y. Jang, *ACS Appl. Mater. Interfaces*, 2011, **3**, 1521–1527.